PNAS
www.pnas.org

Supplementary Information for

Untangling the formation and liberation of water in the lunar regolith

Cheng Zhu[a,b,1], Parker B. Crandall[a,b,1], Jeffrey J. Gillis-Davis[c,2], Hope A. Ishii[c], John P. Bradley[c], Laura M. Corley[c], Ralf I. Kaiser[a,b,2]

[a] Department of Chemistry, University of Hawai'i at Mānoa, Honolulu, HI 96822.

[b] W.M. Keck Laboratory in Astrochemistry, University of Hawai'i at Mānoa, Honolulu, HI 96822.

[c] Hawai'i Institute of Geophysics and Planetology, University of Hawai'i at Mānoa, Honolulu, HI 96822.

[1] C.Z. and P.B.C. contributed equally to this work.

[2] To whom correspondence may be addressed. Email: gillis@higp.hawaii.edu or ralfk@hawaii.edu.

This PDF file includes:

Supplementary Information Text
Figs. S1 to S2
Tables S1 to S3
References for SI reference citations

www.pnas.org/cgi/doi/10.1073/pnas.1819600116

Supplementary Information Text

Experimental Setup. The irradiation experiments were carried out in a contamination-free, ultrahigh vacuum chamber, which is evacuated to 1×10^{-10} Torr by using two magnetically suspended turbo molecular pumps backed by an oil-free scroll pump (1). Typically, 0.8 g of San Carlos olivine powder sieved to grain size less than 45 μm was pressed on a polished silver mirror (3.1×3.1 cm^2). The mineral standard powders are completely anhydrous as no –OH and/or H_2O features (~ 8.6 eV features) were observed in the VEEL spectrum of the sample (Fig. 5). The wafer was interfaced via indium foil for better thermal conductivity to a rotatable oxygen-free high conductivity copper cold finger attached to a two-stage, closed-cycle helium compressor (CTI-Cryogenics Cryodyne 1020, compressor: CTI-Cryogenics 9600). A silicon diode sensor (Lakeshore DT-470) was attached to the cold finger to monitor the temperature of the sample, which was controlled within the range of 10 to 300 K using a Lakeshore 336 temperature controller with an accuracy of ± 0.5 K. Each sample was cooled to 10.0 ± 0.5 K, whereupon it was irradiated by singly charged molecular deuterium ions (D_2^+) generated by a quadruply differentially pumped SPECS IQE 12/38 ion gun (1, 2). A Wien filter quantitatively removed undesired D^+ and D_3^+ ions. It is critical to outline that we chose to implant D_2^+ instead of D^+ because the maximum current of the D^+ generated from the ion gun of 20 ± 2 nA is two orders of magnitude less than ion current of the D_2^+ beam of 2200 ± 200 nA. Hence, to implant $(1.0 \pm 0.1) \times 10^{18}$ cm^{-2} ions, it would take more than 1,300 hours to carry out the experiments. This is beyond the capability of our system to continuously operate under stable conditions for nearly two months.

It shall be noted that previous experimental studies demonstrated that molecular ions such as H_2^+ and even O_2^+ with kinetic energies larger than 1.9 keV and 2.9 keV, respectively, are *completely* dissociated upon interaction with solid surfaces (3, 4). Based on these experimental studies, since the present experiments are conducted with 5 keV D_2^+, the survival probability of D_2^+ *inside* the sample is zero. Only if *low energy* ions such as H_2^+ interact with metal surfaces, an electron can be transferred from the metal to the H_2^+ thus initially generating electronically excited H_2, which is scattered back from the surface into the *gas phase*, but not inside the solid (5-7).

Infrared Laser. Infrared photons (10.6 μm) from a SYNRAD Firestar v40 5 KHz carbon dioxide (CO_2) laser were exploited to simulate micrometeorite impact. In the planetary science community, it is well recognized that a CO_2 laser can effectively melt minerals such as olivine to generate chondrule analogues (8, 9) with microseconds pulse width lasers demonstrated to alter silicate materials (10) and cause lattice disturbance (11). Therefore, although compared to a nanosecond laser, the longer microsecond pulse duration would produce less vaporization, according to our previous experiment, the CO_2 laser is able to heat the sample higher than the partial melting point of Murchison meteorite (above 1400 K) and simulate the thermal effects of micrometeorite impacts.

Calibration Procedure Quadrupole Mass Spectrometer. During the full duration of the experiment, mass spectra of the gas phase species were recorded using a Balzer QMG 422 electron impact quadrupole mass spectrometer (EI-QMS) operating in an electron impact ionization mode at electron impact energies of 100 eV and 0.7 mA emission current. A quantification of the D2-water molecules released into the gas phase during the laser irradiation (Table S3) was conducted via calibrating the mass spectrometer for deuterium molecules (m/z = 4) in separate experiments via a calibrated leak valve, deriving the absolute number of deuterium molecules released during the experiment, and correcting for the ionization cross section of deuterium versus water at 100 eV electron impact energy to calculate the D2-water molecules released into the gas phase. An Accu-Flow Crimped-Capillary Calibrated Leaks for deuterium (Vacuum Technology Incorporated) was interfaced to the main chamber and opened for a well-defined period of t seconds with a defined leak rate of $Q = 1.12 \times 10^{-6}$ torr L s^{-1}. The number of deuterium molecules (n_{D_2}) introduced into the chamber is determined via equation (1) with R and T representing the ideal gas constant (8.314 J mol^{-1} K^{-1}) and temperature (293 K), respectively.

$$n_{D_2} = \frac{\int_0^t Q dt}{RT} \tag{1}$$

The correlation coefficient (k) between the number of deuterium molecules (n_{D_2}) and the ion current for singly ionized molecular deuterium (m/z = 4, I_{D_2}) recorded via the QMS is defined via equation (2):

$$k = \frac{n_{D_2}}{\int_0^t I_{D_2} dt} \tag{2}$$

Based on these considerations, number of deuterium molecules released into the gas phase during the actual experiment (n_{D_2}(IRR)) was derived based on the coefficient (k) and the integrated ion counts at $m/z = 4$ during the actual experiment (I_{D_2}(IRR)) exploiting equation (3):

$$n_{D_2}(IRR) = k \int_0^t I_{D_2}(IRR)dt \tag{3}$$

Considering the total electron impact ionization cross sections of deuterium of 0.939 Å^2 and D2-water of 2.263 Å^2 for 100 eV electrons(12, 13) as well as the pumping speed ratio of the two species (0.8), the D2-water molecules released into the gas phase during the laser irradiation (n_{D_2O}(IRR)) was calculated via equation (4):

$$n_{D_2O}(IRR) = \frac{n_{D_2}(IRR)}{0.8} \times \frac{\int_0^t I_{D_2O}(IRR)dt}{\int_0^t I_{D_2}(IRR)dt} \times \frac{0.939}{2.263} \tag{4}$$

where I_{D_2}(IRR) is the D_2O^+ ion current ($m/z = 20$).

Focused Ion Beam Sample Preparation. Standard FIB section preparation procedures in an FEI Helios 660 dual beam focused ion beam instrument (FIB) were used to create electron-transparent thin sections of olivine grains subjected to irradiation and laser-processing. A protective strap of electron beam-deposited platinum (Pt) followed by ion beam-deposited Pt was first deposited to protect the region of interest during subsequent 30 keV Ga^+-ion milling steps to remove a cross-section of the olivine sample. The section was removed as an approximately 1 µm thick slab and Pt-welded to a copper half-grid where it was further thinned by ion milling to electron transparency (100 nm thickness). The amorphous damaged kerf generated by 30 keV ion milling was removed by a 5 keV ion cleaning step on each side of the final FIB cross-section.

(Scanning) Transmission Electron Microscopy and Spectroscopy. FIB cross-sections were imaged by 300 keV brightfield and high angle annular dark field (HAADF) transmission electron microscopy in an FEI high-base Titan G2 60-300 monochromated and dual aberration-corrected (scanning) transmission electron microscope or (S)TEM. The Titan (S)TEM is equipped with a Gatan Tridiem GIF (Gatan imaging filter) for imaging and spectroscopy. Valence electron energy loss (VEEL) spectra were collected at 300 keV using an incident electron probe 2 Å in diameter and 100 pA probe current with an intrinsic energy resolution of 0.18 eV. To minimize damage to the specimen we used diffraction-coupled, point-count mode, a slightly underfocused

probe and short (3 s) acquisitions. Spectra were acquired from the olivine substrate, multiple locations within the amorphous rim and a brucite ($Mg(OH)_2$) mineral standard.

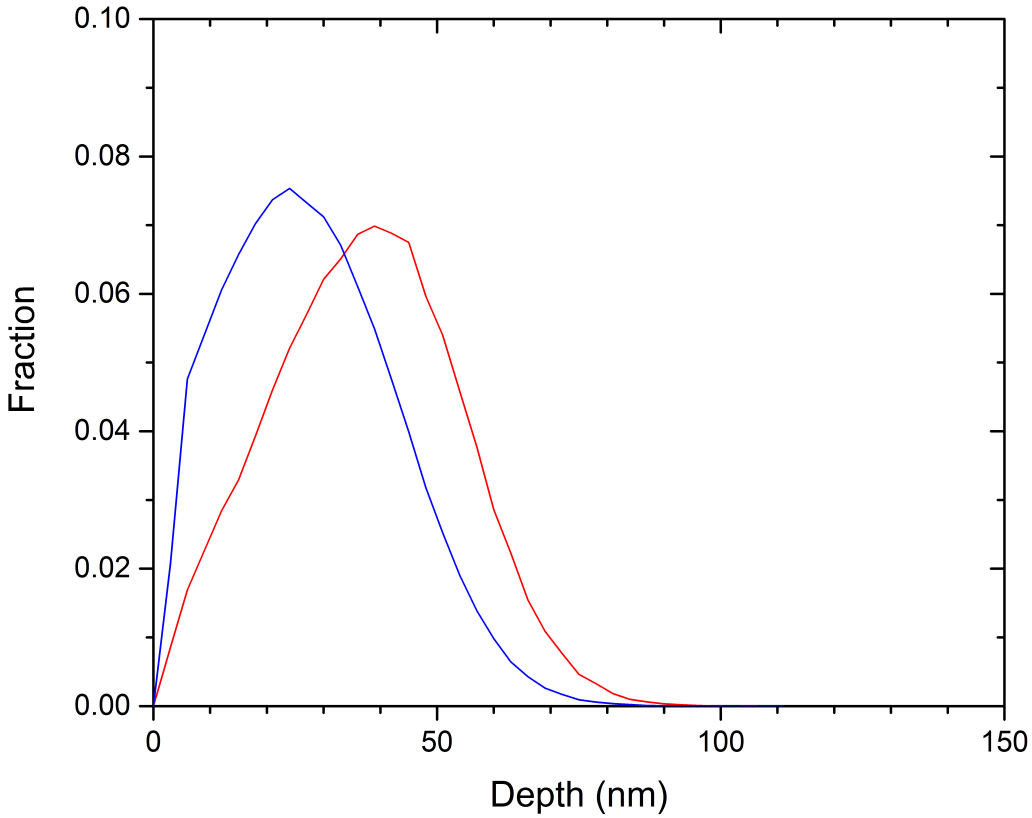

Fig. S1. Calculated implantation profiles from SRIM of 2.5 keV D^+ ions into olivine (red) overlaid by the recoil distribution of the oxygen recoil atoms (blue). The range of the amorphized olivine as determined via imaging of 125 ± 30 nm agrees nicely with the maximum penetration depth of implanted 2.5 keV D^+ ions simulated by SRIM of 100 ± 8 nm. Also, the average penetration depth of the 2.5 keV D^+ ions of 39 ± 4 nm as simulated by SRIM matches well with the existence of 45 ± 5 nm deep pits within olivine.

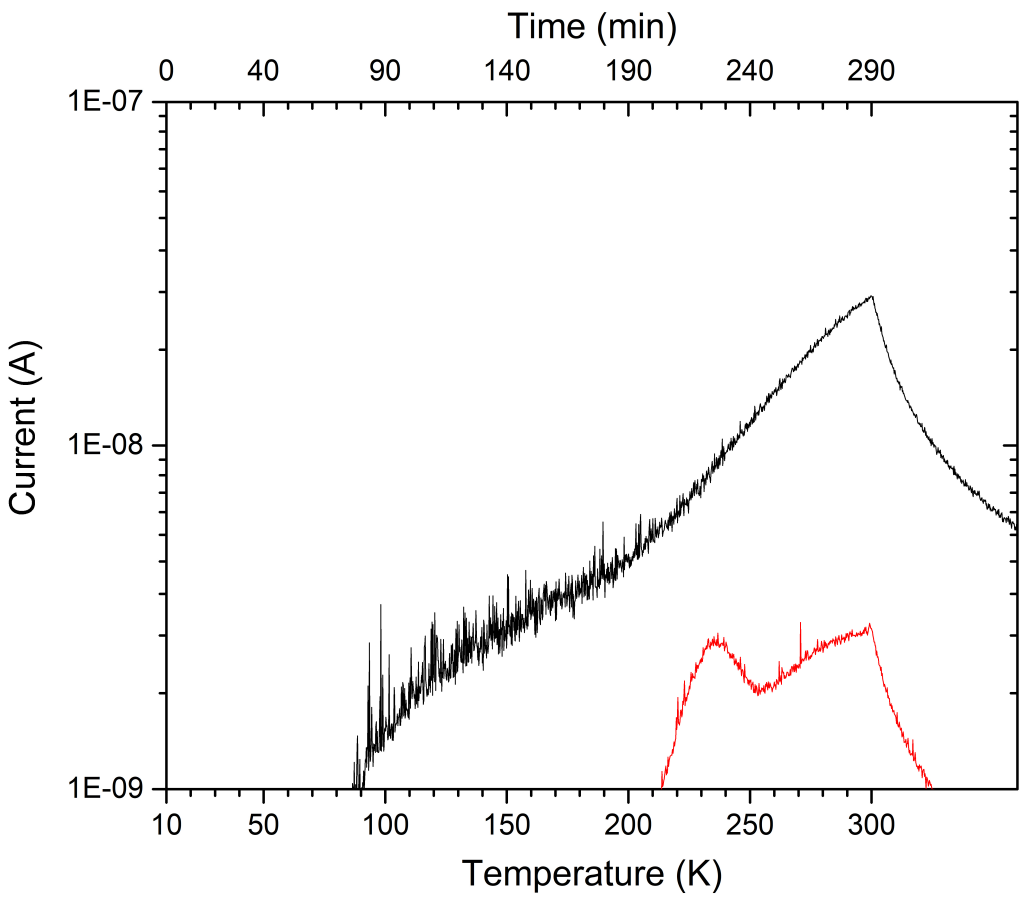

Fig. S2. Quadrupole mass spectrometry profiles recorded at mass-to-charge *m/z* = 4 (D_2^+) during the temperature programmed desorption (TPD) of ion implanted olivine (black) and of ion implanted – laser processed olivine (red). The reduced deuterium storage capability of the laser exposed olivine samples is clearly visible.

Table S1. Summary of experimental sets.

Sources	Stages and parameters				
D_2^+ ion irradiation	D_2^+ ion	TPD			
	10 K, 810 min	10 to 300 K, 290 min			
D_2^+ ion / laser irradiation	D_2^+ ion	Laser Irradiation 1	TPD	Laser Irradiation 2	Laser Irradiation 3
	10 K, 810 min	10 K, 30 min	10 to 300 K, 290 min	300 K, 30 min	300 K, 30 min
D_2 (Blank)	D_2	TPD			
	10 K, 810 min	10 to 300 K, 290 min			
D_2 / laser irradiation (Blank)	D_2	Laser Irradiation 1	TPD	Laser Irradiation 2	Laser Irradiation 3
	10 K, 810 min	10 K, 30 min	10 to 300 K, 290 min	300 K, 30 min	300 K, 30 min

Table S2. Parameters for SRIM simulations and irradiation sources.

	D_2^+ ion gun
Initial energy of the ions (keV)	5
Equivalent deuteron flux (cm^{-2} s^{-1})	$2.0 \pm 0.2 \times 10^{13}$
Irradiated area (cm^2)	1.4 ± 0.2
Irradiation time (min)	810
Total deuteron (cm^{-2})	$(1.0 \pm 0.1) \times 10^{18}$
	CO_2-laser
Wavelength of the laser (μm)	10.6
Laser power (W cm^{-2})	2.4 ± 0.3
Irradiated area (cm^2)[a]	1.0 ± 0.1
Single round irradiation time (min)	30
Total deposited laser energy (J m^{-2})	$(4.3 \pm 0.4) \times 10^7$

[a] Calculated based on the beam diameter at laser output, beam divergence, and the distance between laser output and sample.

Table S3. Number of released deuterium and D2-water molecules during the laser exposure of ion implanted olivine samples.

Species	Laser irradiation 1	Laser irradiation 2	Laser irradiation 3	Total
D_2	$(8.5 \pm 0.8) \times 10^{14}$	$(3.6 \pm 0.4) \times 10^{14}$	$(4.6 \pm 0.5) \times 10^{13}$	$(1.3 \pm 0.1) \times 10^{15}$
D_2O	$(1.0 \pm 0.1) \times 10^{13}$	$(2.3 \pm 0.3) \times 10^{12}$	$(2.3 \pm 0.3) \times 10^{11}$	$(1.3 \pm 0.1) \times 10^{13}$

References

1.Crandall PB, Góbi S, Gillis-Davis J, & Kaiser RI (2017) Can perchlorates be transformed to hydrogen peroxide (H_2O_2) products by cosmic rays on the Martian surface? *J Geophys Res-Planet* 122:1880-1892.

2.Ennis C, Bennett CJ, Jones BM, & Kaiser RI (2011) Formation of D2-water and D2-carbonic acid in oxygen-rich solar system ices via D_2^+ irradiation. *Astrophys J* 733(2):79.

3.Wieser M, Wurz P, Brüning K, & Heiland W (2002) Scattering of atoms and molecules off a magnesium oxide surface. *Nucl Instrum Meth B* 192(4):370-380.

4.Kato S, Tanaka N, Sasao M, Kisaki M, Tsumori K, Nishiura M, Matsumoto Y, Kenmotsu T, Wada M, & Yamaoka H (2015) Angle-resolved intensity and energy distributions of positive and negative hydrogen ions released from tungsten surface by molecular hydrogen ion impact. *J Nucl Mater* 463:351-354.

5.Müller H, Hausmann R, Brenten H, & Kempter V (1993) Electrons from ultra-and interatomic Auger processes in low-energy grazing collisions of H^+ and H_2^+ with W(110) partially covered by alkali atoms. *Surf Sci* 284(1-2):129-138.

6.Lorente N, Teillet-Billy D, & Gauyacq J-P (1999) H_2^+ scattered off Al surfaces: The role of the negative ion resonance $^2\Sigma_u^+$. *J Chem Phys* 111(15):7075-7083.

7.Krischok S, Müller H, & Kempter V (1999) Surface induced dissocation in slow collisions of H_2^+ and O_2^+: information from the ion impact electron spectra. *Nucl Instrum Meth B* 157(1-4):198-207.

8.Cervantes-de la Cruz KE, Gutiérrez FO, Viñas JS, Peralta AS, Salas MAR, García BSÁ, del Consuelo Macías Romo M, & Linares-López C (2015) Experimental chondrules by melting samples of olivine, clays and carbon with a CO_2 laser. *Bol Soc Geol Mex* 67(3):401-412.

9.Beitz E, Blum J, Mathieu R, Pack A, & Hezel DC (2013) Experimental investigation of the nebular formation of chondrule rims and the formation of chondrite parent bodies. *Geochim Cosmochim Ac* 116:41-51.

10.Moroz L, Fisenko A, Semjonova L, Pieters C, & Korotaeva N (1996) Optical effects of regolith processes on S-asteroids as simulated by laser shots on ordinary chondrite and other mafic materials. *Icarus* 122(2):366-382.

11.Kissel J & Krueger F (1987) Ion formation by impact of fast dust particles and comparison with related techniques. *Appl Phys A* 42(1):69-85.

12. Straub H, Lindsay B, Smith K, & Stebbings R (1998) Absolute partial cross sections for electron-impact ionization of H_2O and D_2O from threshold to 1000 eV. *J Chem Phys* 108(1):109-116.
13. Yoon J-S, Kim Y-W, Kwon D-C, Song M-Y, Chang W-S, Kim C-G, Kumar V, & Lee B (2010) Electron-impact cross sections for deuterated hydrogen and deuterium molecules. *Rep Prog Phys* 73(11):116401.